

Advection Dominated Accretion Flows in the Kerr Metric: I. Basic Equations

Charles F. Gammie¹ and Robert Popham
Harvard-Smithsonian Center for Astrophysics, MS-51
60 Garden St., Cambridge, MA 02138

September 3, 2018

ABSTRACT

We write down and solve equations describing steady state, optically thin, advection-dominated accretion onto a Kerr black hole. The mean flow, described by the relativistic fluid equations, is axisymmetric and vertically averaged. The effect of turbulence in the flow is represented by a viscous shear stress. Our treatment differs in several important ways from earlier work: we use a causal prescription for the shear stress, we do not assume the relativistic enthalpy is unity (this is important for rapidly rotating holes), and we use a relativistic equation of state. We present several representative solutions and use them to evaluate the importance of relativistic effects, to check our approximations, and to evaluate the robustness of the input physics. Detailed properties of the solutions are described in an accompanying paper.

1. Introduction

The structure of accretion flows close to the horizon of a black hole is of considerable astrophysical interest because: (1) most of the gravitational binding energy is released close to the black hole; (2) there are strong-field gravitational effects close to the horizon that are unique to black holes; (3) temperatures are highest close to the horizon, so exotic physical processes may occur there.

Early studies of disk accretion onto black holes assumed a thin disk. Shakura & Sunyaev (1973) presented the basic equations used to describe thin disks, but did not include relativity. Accretion in thin, relativistic disks was first described by Bardeen, Press, & Teukolsky (1972) and Novikov & Thorne (1973). Note that recently Riffert & Herold (1995) corrected an algebraic error in NT's version of the vertical structure equation.

¹also Institute of Astronomy, Madingley Road, Cambridge CB3 0HA, United Kingdom

Paczyński & Bisnovatyi-Kogan (1981), Muchotrzeb & Paczyński (1982), and Abramowicz et al. (1988) introduced a set of disk equations, dubbed the “slim disk” equations by Abramowicz et al. (1988), which include a number of terms neglected in the thin disk formulation. These equations include radial pressure gradient, acceleration, and energy transport, and provide the basis for the equations used in this paper and most of the other recent work cited here on disk structure around black holes. These studies all used the “Paczyński potential”, a pseudo-relativistic potential designed to reproduce the main features of orbits around a nonrotating black hole (Paczyński & Wiita (1980)).

One of the terms included in the slim disk equations is the inward advection of entropy by the accreting gas. Narayan & Popham (1993) showed that this term, which is insignificantly small in the usual thin disk, becomes large in the optically thin boundary layer region of low-accretion rate cataclysmic variables. Narayan and Yi recognized the existence of a class of flows in which advection dominates the energy balance, and found a self-similar solution in the advection-dominated limit (Narayan & Yi (1994), Narayan & Yi (1995a)). Advection-dominated solutions were recognized as a new class of thermal equilibria (Abramowicz et al. (1995), Chen et al. (1995), Narayan & Yi (1995b)). They resemble some earlier models by Rees et al. (1982) and Begelman & Meier (1982), where the hot accreting gas radiates very inefficiently.

In this paper we concentrate on a particular class of flows: optically thin, advection-dominated accretion flows, or ADAFs. These flows cool slowly, so most of the heat deposited in them by the dissipation of turbulence (which also carries off angular momentum) is advected into the black hole rather than radiated away. The accretion is therefore inefficient compared to a thin disk, which can radiate away a substantial fraction of the accreted rest mass energy. Over the past few years, the theory of these flows has been developed and applied to a number of observed black hole systems (see Narayan (1997) for a review). Most recently, Narayan, Kato, & Honma (1997) (NKH) and Chen, Abramowicz, & Lasota (1997) presented global, advection-dominated disk solutions in the Paczyński potential. Our work differs from this in that it is fully relativistic, and includes effects due to strong rotation of the black hole.

Recently, a number of authors have included the effects of relativity in their models of disks around black holes. Lasota (1994) first wrote down slim disk equations which included relativistic effects. This was superseded by the work of Abramowicz et al. (1997) (ACGL), who corrected some errors in Lasota’s work and provided sample numerical solutions. Our work differs from this one in many details, but mainly in our use of a turbulent stress prescription that is explicitly related to the Navier-Stokes stress and that is causal, and in our inclusion of the relativistic enthalpy. Abramowicz, Lanza, & Percival (1997) (ALP)

revisited the question of vertical structure and derived a new expression for the scale height beginning with the Euler equations. We adopt ALP’s version of the vertical structure equations, with a minor correction. Independently, Peitz & Appl (1997) (PA) gave a very nice and rather complete treatment of the problem, which included a causal viscosity and the relativistic enthalpy; however, they used a polytropic equation of state rather than solving the energy equation as we do. Chakrabarti (1996) has also considered rotating accretion flows in the Kerr metric, but only in the weak viscosity limit. Also, unlike all of the above, we use a relativistic equation of state. This correction increases in importance as the hole rotates more and more rapidly. Finally, we correct some minor errors in some of the above treatments.

The spirit of this work is to do the best possible job on the physics, including the relativity and turbulent shear stress, within certain limitations. One limitation is physical: there is no well justified formalism for treating the effects of turbulence in these flows. We treat the mean flow using the full equations of relativistic hydrodynamics, and include the effects of turbulence via a turbulent shear stress, making the minimal modifications of the inviscid equations necessary to allow angular momentum transport and therefore accretion. Another limitation is complexity: we are forced to make some approximations simply because without them the equations would be too difficult to solve. Despite these limitations, this work reveals some generic properties of relativistic ADAFs, and, when coupled with a proper scheme for relativistic photon transport, will allow us to model their observational appearance.

The plan of this paper is as follows. In §2 we explain our units, notation, and record the relevant metrics and frames. In §3 we write down the basic dynamical equations. In §4 we consider the heart of the physics in this problem, the turbulent shear stress. In §5 we evaluate the critical point conditions. In §6 we give a sample solution (a full survey of solutions is described in Popham & Gammie (1997)), and evaluate our approximations. §7 contains our conclusions.

2. Preliminaries

2.1. Units and Metric

We adopt $G = M = c = 1$ as our basic scalings, where M is the black hole mass. This implies a unit of mass, length, and time of M , GM/c^2 , and GM/c^3 , respectively. The angular momentum J of the black hole is described by $a \equiv Jc/GM^2$, where $-1 < a < 1$. It is convenient to define, like NT, the following relativistic correction factors that become

unity in the nonrelativistic limit:

$$\mathcal{A} \equiv 1 + a^2/r^2 + 2a^2/r^3, \quad (1)$$

$$\mathcal{C} \equiv 1 - 3/r + 2a/r^{3/2}, \quad (2)$$

$$\mathcal{D} \equiv 1 - 2/r + a^2/r^2, \quad (3)$$

and

$$\mu \equiv 1 + a^2 \cos^2 \theta / r^2. \quad (4)$$

In Boyer-Lindquist coordinates, the Kerr metric is

$$ds^2 = -(1 - \frac{2}{r\mu})dt^2 - \frac{4a \sin^2 \theta}{r\mu} dt d\phi + \frac{\mu}{\mathcal{D}} dr^2 + r^2 \mu d\theta^2 + \quad (5)$$

$$r^2 \sin^2 \theta \left(1 + \frac{a^2}{r^2} + \frac{2a^2 \sin^2 \theta}{r^3 \mu}\right) d\phi^2. \quad (6)$$

The non-zero contravariant components are

$$\begin{aligned} g^{tt} &= -1 - 2(1 + a^2/r^2)/r\mathcal{D}\mu, & g^{t\phi} &= -2a/r^3\mathcal{D}\mu, & g^{rr} &= \mathcal{D}/\mu, \\ g^{\theta\theta} &= 1/r^2\mu, & g^{\phi\phi} &= (1 - 2/r\mu)/r^2 \sin^2 \theta \mathcal{D}. \end{aligned} \quad (7)$$

Often we shall only require the metric in the equatorial plane, where

$$ds^2 = -\frac{\mathcal{D}}{\mathcal{A}} dt^2 + r^2 \mathcal{A} (d\phi - \omega dt)^2 + \frac{1}{\mathcal{D}} dr^2, \quad (8)$$

and

$$\omega \equiv \frac{2a}{\mathcal{A}r^3} \quad (9)$$

measures the rate of frame dragging by the hole. In expanded form,

$$ds^2 = -(1 - \frac{2}{r})dt^2 - \frac{4a}{r} dt d\phi + \frac{1}{\mathcal{D}} dr^2 + r^2 \mathcal{A} d\phi^2. \quad (10)$$

The nonzero contravariant components of the metric in the equatorial plane are

$$g^{tt} = -\mathcal{A}/\mathcal{D}, \quad g^{t\phi} = -2a/r^3\mathcal{D}, \quad g^{rr} = \mathcal{D}, \quad g^{\phi\phi} = (1 - 2/r)/r^2\mathcal{D}. \quad (11)$$

In the equatorial plane, the horizon lies at the outer root of $\mathcal{D} = 0$, i.e. $r = 1 + \sqrt{1 - a^2}$. The boundary of the “ergosphere”, where the world lines of observers at constant Boyer-Lindquist coordinates (r, θ, ϕ) become spacelike (and therefore unphysical) lies at $r = 2$ in the equatorial plane.

2.2. Basic Flow Symmetry, Vertical Averaging

Our goal is to accurately describe the flow of fluid in the highly relativistic regime, close to the horizon. To do so we must make some simplifying assumptions. First, we assume the angular momentum of the accreting fluid is aligned with the angular momentum of the black hole.² Second, we assume that the flow, described by its four-velocity $(u^t, u^r, u^\theta, u^\phi)$ is in the mean axisymmetric and symmetric about the equatorial plane. Then u_θ vanishes at the equatorial plane.

We also vertically average the flow, a standard approximation in accretion flows with angular momentum. This is best explained by example. Consider the particle number conservation equation:

$$(\rho u^\mu)_{;\mu} = 0. \quad (12)$$

Here ρ is the “rest-mass density”. Then

$$(\rho u^\mu)_{;\mu} = \frac{1}{\sqrt{g}}(\sqrt{g}u^\mu)_{,\mu} = \frac{1}{r^2}(r^2\rho u^r)_{,r} + \frac{1}{\mu \sin \theta}(\mu \sin \theta u^\theta)_{,\theta} = 0, \quad (13)$$

where $g = |\text{Det}(g_{\mu\nu})| = r^4 \sin^2 \theta \mu^2$.

We now perform a “vertical” average by integrating over the volume between r and $r + \delta r$. Then the second term in equation (13) vanishes. Now define H_θ , the characteristic angular scale of the flow about the equator, and assume this to be the same for all flow variables f . The vertical averaging approximation consists in taking

$$\int d\theta d\phi \sqrt{g} f \simeq 4\pi H_\theta f(\theta = \pi/2), \quad (14)$$

whence

$$(4\pi H_\theta r^2 \rho u^r)_{,r} = 0. \quad (15)$$

Integrating once in radius,

$$4\pi H_\theta r^2 \rho u^r = -\dot{M}, \quad (16)$$

where the constant \dot{M} is the “rest-mass accretion rate”.

² We make this assumption because the full non-aligned problem is intractable. Alignment of the flow due to gravitomagnetic precession and viscosity (the Bardeen-Petterson effect, see Bardeen & Petterson (1975), Kumar & Pringle (1985)) is not likely to be important for the hot flows considered here.

2.3. Frames

We use four separate frames in our calculations. The first and most important is the Boyer-Lindquist coordinate frame (BLF), where most direct calculations are done.

Second is the locally nonrotating frame (LNRF), an orthonormal tetrad basis carried by observers who live at constant θ and r , but at $\phi = \omega t + \text{const.}$, so they are dragged in azimuth by the black hole. Their world lines are always timelike, even in the ergosphere. Explicit transformations between the LNRF and BLF are given by Bardeen, Press, & Teukolsky (1972).

A third frame is obtained by an azimuthal Lorentz boost from the LNRF into another tetrad basis that corotates with the fluid (the corotating frame, or CRF). The CRF has velocity β_ϕ with respect to the LNRF; we also define $\gamma_\phi \equiv (1 - \beta_\phi^2)^{-1/2}$.

Finally we have the local rest frame (LRF) of the fluid, obtained by a radial Lorentz boost from the CRF. The LRF has radial velocity $V < 0$ with respect to the CRF, so we define $\beta_r \equiv V$ and $\gamma_r \equiv (1 - \beta_r^2)^{-1/2}$.

Two velocity variables are needed to describe the flow in the equatorial plane. We choose V (as do ACGL), the radial velocity of the fluid measured in the CRF, and $l \equiv u_\phi$ (as do PA), the angular momentum.

All the contravariant and covariant components of the velocity field can now be expressed in terms of l and V . We find, using $\gamma \equiv \gamma_\phi \gamma_r$,

$$(u_t, u_r, u_\theta, u_\phi) = \left(-\gamma \sqrt{\frac{\mathcal{D}}{\mathcal{A}}} - l\omega, \quad \frac{V}{\sqrt{\mathcal{D}(1-V^2)}}, \quad 0, \quad l \right), \quad (17)$$

$$(u^t, u^r, u^\theta, u^\phi) = \left(\gamma \sqrt{\frac{\mathcal{A}}{\mathcal{D}}}, \quad V \sqrt{\frac{\mathcal{D}}{1-V^2}}, \quad 0, \quad \frac{l}{r^2 \mathcal{A}} + \omega \gamma \sqrt{\frac{\mathcal{A}}{\mathcal{D}}} \right). \quad (18)$$

In terms of l and V ,

$$\gamma^2 = \frac{1}{1-V^2} + \frac{l^2}{r^2 \mathcal{A}}, \quad (19)$$

$$\beta_\phi = \frac{l}{r \sqrt{\mathcal{A}} \gamma}. \quad (20)$$

Recall that $\mathcal{E} \equiv -u_t$ is the “energy at infinity”, and that l and \mathcal{E} are conserved along geodesics.

Finally, it is useful to have explicit expressions for the LRF basis vectors. The

contravariant basis vectors are

$$e^\mu_{(t)} = \left(\gamma \sqrt{\frac{\mathcal{A}}{\mathcal{D}}}, \quad \beta_r \gamma_r \sqrt{\mathcal{D}}, \quad 0, \quad \frac{2a\gamma}{r^3 \sqrt{\mathcal{A}\mathcal{D}}} + \frac{\beta_\phi \gamma}{r \sqrt{\mathcal{A}}} \right) \quad (21)$$

$$e^\mu_{(r)} = \left(\beta_r \gamma \sqrt{\frac{\mathcal{A}}{\mathcal{D}}}, \quad \gamma_r \sqrt{\mathcal{D}}, \quad 0, \quad \frac{2a\beta_r \gamma}{r^3 \sqrt{\mathcal{A}\mathcal{D}}} + \frac{\beta_r \beta_\phi \gamma}{r \sqrt{\mathcal{A}}} \right) \quad (22)$$

$$e^\mu_{(\theta)} = \left(0, \quad 0, \quad \frac{1}{r}, \quad 0 \right) \quad (23)$$

$$e^\mu_{(\phi)} = \left(\beta_\phi \gamma_\phi \sqrt{\frac{\mathcal{A}}{\mathcal{D}}}, \quad 0, \quad 0, \quad \frac{2a\beta_\phi \gamma_\phi}{r^3 \sqrt{\mathcal{A}\mathcal{D}}} + \frac{\gamma_\phi}{r \sqrt{\mathcal{A}}} \right). \quad (24)$$

The covariant basis vectors are

$$e_\mu^{(t)} = \left(\gamma \sqrt{\frac{\mathcal{D}}{\mathcal{A}}} + \frac{2a\beta_\phi \gamma}{r^2 \sqrt{\mathcal{A}}}, \quad -\frac{\beta_r \gamma_r}{\sqrt{\mathcal{D}}}, \quad 0, \quad -\beta_\phi \gamma_r \sqrt{\mathcal{A}} \right) \quad (25)$$

$$e_\mu^{(r)} = \left(-\beta_r \gamma \sqrt{\frac{\mathcal{D}}{\mathcal{A}}} - \frac{2a\beta_r \beta_\phi \gamma}{r^2 \sqrt{\mathcal{A}}}, \quad \frac{\gamma_r}{\sqrt{\mathcal{D}}}, \quad 0, \quad \beta_\phi \beta_r \gamma_r \sqrt{\mathcal{A}} \right) \quad (26)$$

$$e_\mu^{(\theta)} = \left(0, \quad 0, \quad r, \quad 0 \right) \quad (27)$$

$$e_\mu^{(\phi)} = \left(-\beta_\phi \gamma_\phi \sqrt{\frac{\mathcal{D}}{\mathcal{A}}} - \frac{2a\gamma_\phi}{r^2 \sqrt{\mathcal{A}}}, \quad 0, \quad 0, \quad \gamma_\phi r \sqrt{\mathcal{A}} \right) \quad (28)$$

Recall that the basis vectors allow one to transform back and forth from the LRF via $v_{(a)} = e^\mu_{(a)} v_\mu$ and $v_\mu = e_\mu^{(a)} v_{(a)}$.

3. Basic Dynamical Equations

The basic equations of relativistic, viscous hydrodynamics are the energy-momentum conservation equations

$$T^{\mu\nu}{}_{;\nu} = 0, \quad (29)$$

and the particle number conservation, or continuity, equation:

$$(\rho u^\mu)_{;\mu} = 0. \quad (30)$$

We adopt the convention that ρ is the ‘‘rest mass density’’ and u is the internal energy per unit proper volume, so the total density of mass-energy is $\rho + u$. We also define the pressure p and the relativistic enthalpy $\eta \equiv (\rho + u + p)/\rho$. Then the stress-energy tensor is

$$T^{\mu\nu} = p g^{\mu\nu} + \rho \eta u^\mu u^\nu + t^{\mu\nu}, \quad (31)$$

where $t^{\mu\nu}$ is the “viscous” stress-energy tensor. It includes terms due to small-scale velocity and magnetic field fluctuations. We neglect contributions to the stress-energy tensor from the energy flux and from large-scale electromagnetic fields such as those found in MHD winds.

In relativistic Navier-Stokes flow with zero bulk viscosity

$$t^{\mu\nu} = -2\lambda\sigma^{\mu\nu}, \quad (32)$$

where λ is the “coefficient of dynamic viscosity”,³ and

$$\sigma_{\alpha\beta} = \frac{1}{2} \left(u_{\alpha;\mu} h_{\beta}^{\mu} + u_{\beta;\mu} h_{\alpha}^{\mu} \right) - \frac{1}{3} \Theta h_{\alpha\beta}, \quad (33)$$

is the shear tensor. Here

$$\Theta \equiv u^{\alpha}{}_{;\alpha}, \quad (34)$$

and

$$h^{\alpha\beta} \equiv g^{\alpha\beta} + u^{\alpha} u^{\beta} \quad (35)$$

is the projection tensor. Our turbulent shear stress tensor does not have this form, that is, it is not a relativistic Navier-Stokes viscous stress tensor. Instead we write down a turbulent stress tensor, described in §4, that is both the minimal departure from the inviscid equations that allows angular momentum transport and the simplest form that preserves causality.

3.1. Particle Number Conservation

As already discussed, the particle number conservation equation can be reduced to the form

$$-4\pi r^2 \rho u^r H_{\theta} = \dot{M}. \quad (36)$$

Expressing u^r in terms of the preferred dependent variable V ,

$$4\pi r^2 \rho H_{\theta} V \left(\frac{\mathcal{D}}{1-V^2} \right)^{1/2} = -\dot{M}. \quad (37)$$

A closely related equation may be derived with the aid of the Killing vector $\xi_t^{\mu} = (1, 0, 0, 0)$. Then

$$(T^{\nu}{}_{\mu} \xi_t^{\mu})_{;\nu} = 0 = \frac{1}{r^2} (r^2 T^r{}_t)_{,r} + \frac{1}{\mu \sin \theta} (\mu \sin \theta T^{\theta}{}_t)_{,\theta}. \quad (38)$$

³See Israel (1972) for a discussion of relativistic microscopic viscosity.

Vertically averaging, the second term vanishes. Then integrating once in r and expanding we find

$$4\pi H_\theta r^2 [-(\rho + u + p)\mathcal{E}u^r + t_t^r] = \dot{E}. \quad (39)$$

This equation expresses the constancy of mass-energy flux \dot{E} with radius; \dot{E} is the actual rate of change of the black hole mass. If the flow is cold and slow at large radius, $\dot{E} \approx \dot{M}$.

Subtracting equation (36) from equation (39) then dividing by equation (36) gives the following relation:

$$-\frac{t_t^r}{\rho u^r} + \mathcal{E} - 1 + \left(\frac{u + p}{\rho}\right)\mathcal{E} = \frac{\dot{E} - \dot{M}}{\dot{M}}. \quad (40)$$

This reduces to the Bernoulli equation in the inviscid limit.

3.2. Energy Equation

The energy equation is the component of equation (29) parallel to the fluid four-velocity:

$$u_\mu T^{\mu\nu}{}_{;\nu} = 0. \quad (41)$$

Using standard manipulations (e.g. Ellis (1971)), this can be reduced to

$$u^r \frac{du}{dr} - u^r \frac{(u + p)}{\rho} \frac{d\rho}{dr} = \Phi - \Lambda \quad (42)$$

where, provided that $t^{\mu\nu}$ is trace-free, as we shall assume,

$$\Phi = -t^{\mu\nu}\sigma_{\mu\nu} \quad (43)$$

is the dissipation function and Λ is the cooling function.

Two variables are required to represent the thermodynamic state of the fluid. We choose ρ , the rest-mass density, and the scaled temperature T . In dimensional form, T is related to the ordinary kinetic temperature T_K by $T \equiv kT_K/\bar{m}c^2$, where k is Boltzmann's constant and \bar{m} is the mean molecular weight.

The pressure is given by the ideal gas equation of state $p = \rho T$. We fold the magnetic contribution to the pressure into p and any magnetic contribution to the energy per unit proper volume into the internal energy u . We must now specify $u(\rho, T)$. We require an equation of state that is polytropic in the nonrelativistic limit with adiabatic index γ_o . Since the magnetic energy is included in the internal energy, γ_o may differ from 5/3. Thus we set

$$u = \rho T g(T) \equiv \rho T \left(\frac{4/(\gamma_o - 1) + 15T}{4 + 5T} \right). \quad (44)$$

This formula fits the exact relativistic equation of state for an ideal relativistic Boltzmann gas (see, e.g., Service (1986)), for which $\gamma_o = 5/3$, to everywhere better than 2%.⁴ The sound speed is then

$$c_s^2 = \frac{\Gamma p}{\eta \rho} = \frac{\Gamma T}{\eta}, \quad (45)$$

where

$$\Gamma \equiv \left. \frac{\partial \ln p}{\partial \ln \rho} \right|_s = 1 + \frac{1}{g + T(dg/dT)}. \quad (46)$$

When $\gamma_o = 5/3$, our Γ agrees with Service's to within 0.5%, and our sound speed agrees with hers to within 1.3%.

The energy equation can now be reduced to

$$V \left(\frac{\mathcal{D}}{1 - V^2} \right)^{1/2} \left(\frac{\partial u}{\partial T} \frac{dT}{dr} - \frac{p}{\rho} \frac{d\rho}{dr} \right) = \Phi - \Lambda. \quad (47)$$

The dissipation function can be evaluated once we specify the viscous stress.

Like NKH, we do not include cooling explicitly, but set $\Phi - \Lambda = f\Phi$, where $f \leq 1$ is a constant factor that we vary to estimate the effect of cooling. Our energy equation is essentially the same as ACGL, except that we include the relativistic equation of state, and our dissipation function is different. PA do not solve an energy equation; instead they use a polytropic equation of state.

3.3. Radial Momentum

The radial momentum equation is the radial component of the projection of equation (29) into the space normal to the four-velocity:

$$h_{r\mu}(T^{\mu\nu})_{;\nu} = 0. \quad (48)$$

Using standard manipulations (we must evaluate some connection coefficients), and neglecting the viscous acceleration, the radial momentum equation becomes

$$\frac{V}{1 - V^2} \frac{dV}{dr} = f_r - \frac{1}{\rho\eta} \frac{dp}{dr}, \quad (49)$$

⁴ An even better fit to the ideal relativistic Boltzmann gas equation of state is $g(T) = (12 + 45T + 45T^2)/(8 + 20T + 15T^2)$, which has a maximum relative error of 7×10^{-4} .

where

$$f_r \equiv -\frac{1}{r^2} \frac{\mathcal{A}\gamma_\phi^2}{\mathcal{D}} \left(1 - \frac{\Omega}{\Omega_+}\right) \left(1 - \frac{\Omega}{\Omega_-}\right) \quad (50)$$

and $\Omega \equiv u^\phi/u^t = \omega + l\mathcal{D}^{1/2}/r^2\mathcal{A}^{3/2}\gamma$, and $\Omega_\pm = \pm(r^{3/2} \pm a)^{-1}$ is the rotation frequency, as observed at large radius, of circular, planar orbits.

Our radial momentum equation obviously reduces correctly to the nonrelativistic limit. It agrees with PA's radial momentum equation, although theirs is expressed in different variables. It also agrees with ACGL's, although ACGL take $\eta = 1$.

3.4. Angular Momentum

An angular momentum equation can be derived with the aid of the azimuthal Killing vector $\xi_\phi^\mu = (0, 0, 0, 1)$. We have

$$(T^\nu{}_\mu \xi_\phi^\mu)_{;\nu} = 0 = (T^\nu{}_\phi)_{;\nu} = \frac{1}{\sqrt{g}} (\sqrt{g} T^\nu{}_\phi)_{;\nu} = \frac{1}{r^2} (r^2 T^r{}_\phi)_{;r} + \frac{1}{\mu \sin \theta} (\mu \sin \theta T^\theta{}_\phi)_{;\theta}. \quad (51)$$

Vertically averaging, the second term vanishes, and integrating once and using the definition of the stress tensor, we obtain

$$\dot{M}l\eta - 4\pi H_\theta r^2 t^r{}_\phi = \dot{M}j. \quad (52)$$

Here $\dot{M}j$ is the total inward flux of angular momentum; j is treated as an eigenvalue of the problem and must be self-consistently obtained.

Our angular momentum equation agrees with PA and ACGL, except that ACGL assume $\eta = 1$.

3.5. Vertical Structure

We assume vertical equilibrium, and use the expression for the simplified equilibrium scale height derived by ALP under the assumption that u^θ and $u^\theta{}_{;\theta}$ are small. A convenient way to express ALP's result is to define an effective vertical frequency via

$$H_\theta^2 = \frac{p}{\rho\eta r^2 \nu_z^2}. \quad (53)$$

Then ALP find ⁵

$$\nu_z^2 = \frac{l^2 - a^2(\mathcal{E}^2 - 1)}{r^4}. \quad (54)$$

In the limit of a relativistic, thin disk this reduces to $\nu_z^2 = r^{-3}(1 - 4a/r^{3/2} + 3a^2/r^2)/\mathcal{C}$, which agrees with the result of Riffert & Herold (1995), and obviously reduces correctly to the nonrelativistic limit.

ALP’s result for the equilibrium scale height differs from PA’s. The reason is that ALP neglect u^θ and its derivatives, while PA work in a quasi-cylindrical coordinate system (t, r, z, ϕ) and thus neglect u^z and its derivatives. The two assumptions are not equivalent. If the flow is quasi-spherical, then ALP’s approach is superior.

The major defect of all these approaches to vertical structure is that they assume vertical equilibrium. This assumption is not justified close to the event horizon. Inflow there is so rapid that inertial terms become important, and the scale height effectively “freezes out.” ALP provide an expression for the evolution of the scale height that takes this effect into account, but we have not used this because it introduces significant mathematical complications.

4. Turbulent Shear Stress

The key to calculating the structure of steady, rotating accretion flows lies in understanding the nature of the viscous stress t^r_ϕ that allows the angular momentum of the flow to evolve. In our view the viscous stress is likely caused by MHD turbulence initiated by the Balbus-Hawley instability (Balbus & Hawley (1991)). In this case, the “viscous” stress is really a time-averaged turbulent Reynolds and Maxwell stress (see Balbus, Gammie, & Hawley (1994)).

The viscous stress is commonly assumed to have the Navier-Stokes form (see eq. [32]). One difficulty with this assumption is that, as pointed out by Narayan (1992), the resulting system of equations are acausal: they propagate information at infinite speed. This has the undesirable consequence that one must apply a boundary condition at the event horizon (e.g. Narayan, Kato, & Honma (1997)).

Various workers have sought to remedy this defect, including Narayan (1992), Narayan,

⁵ This expression is closely related to a well-known integral of the motion for geodesics in the Kerr geometry: $Q = u_\theta^2 + \cos^2\theta \left(\frac{l^2}{\sin^2\theta} - a^2(\mathcal{E}^2 - 1) \right)$ [Carter (1968)]. In the limit of small $\delta\theta = \theta - \pi/2$, $Q \simeq u_\theta^2 + r^4\delta\theta^2\nu_z^2$. Evidently Q is proportional to a vertical energy of oscillation.

Loeb, & Kumar (1994), Papaloizou & Szuszkiewicz (1994) (hereafter PS), Kato & Inagaki (1994), Kato (1994), and Narayan (1996, private communication). We follow PS’s line of reasoning because it is straightforward to generalize it to the relativistic case.

4.1. Causal Viscosity: Nonrelativistic Case

PS introduce a phenomenological equation for the evolution of the viscous stress that allows it to relax toward an equilibrium value. Let us review their result in our notation, temporarily assuming that the velocities are nonrelativistic and the geometry is Euclidean. Then PS’s equation for the viscous stress $S = t^r_\phi$ is

$$\frac{DS}{D\tau} = -\frac{S - S_o}{\tau_r}, \quad (55)$$

where $D/D\tau$ is the convective derivative, S_o is the equilibrium value of the stress and τ_r is the relaxation timescale. In a steady state

$$V \frac{dS}{dr} = -\frac{S - S_o}{\tau_r}. \quad (56)$$

Now take d/dr of the angular momentum equation to obtain

$$\frac{\dot{M}}{2\pi} \frac{dl}{dr} = 2H_\theta \left(2rS + r^2 \frac{dS}{dr} \right), \quad (57)$$

neglecting terms of order dH_θ/dr . Solve for dS/dr in equation(57), eliminate dS/dr from equation(56), and use $S_o = -\rho\nu r^2 d\Omega/dr$ to find

$$S = \frac{\rho\nu r}{1 - 2\tau V/r} \left(-r \frac{d\Omega}{dr} + \frac{V^2}{c_\nu^2} \frac{1}{r} \frac{dl}{dr} \right), \quad (58)$$

where $c_\nu = \sqrt{\nu/\tau_r}$ is the speed at which viscous effects propagate (see the discussion of PS). If $\tau_r \simeq \Omega^{-1}$ (as one might expect for Balbus-Hawley induced turbulence), and $\nu \simeq \alpha c_s^2/\Omega$, then $c_\nu \simeq c_s \alpha^{1/2}$. Rewriting equation(58) slightly,

$$S = \frac{\rho\nu r}{1 - 2\tau V/r} \left[-\frac{1}{r} \frac{dl}{dr} \left(1 - \frac{V^2}{c_\nu^2} \right) + \frac{2l}{r^2} \right]. \quad (59)$$

Evidently this viscosity prescription introduces a singular point into the angular momentum equation at $V^2 = c_\nu^2$, since the coefficient of dl/dr in the angular momentum equation vanishes there. This requires a new boundary condition at the singular point. The new boundary condition replaces the old, objectionable boundary condition at the surface of the accreting object.

4.2. Causal Viscosity: Relativistic Case

We now generalize PS's causal stress prescription to the relativistic case. Begin with the viscous stress-energy tensor measured in the LRF, $t_{(a)(b)}$. We assume that all components vanish except $t_{(r)(\phi)} = t_{(\phi)(r)}$. This is the minimal modification of the inviscid equations that produces angular momentum transport. Notice that the LRF is the only safe place to make such modifications, since an arbitrary modification of the stress tensor in another frame can have unintended side effects. Then, with the aid of equations (26) and (28), we find ⁶

$$t^r{}_{\phi} = \gamma r \sqrt{\mathcal{A}\mathcal{D}} t_{(r)(\phi)} \equiv F t_{(r)(\phi)}. \quad (60)$$

We now identify $t_{(r)(\phi)}$ with S , the component of the stress that obeys the relativistic analogue of equation (55):

$$\frac{DS}{D\tau} = -\frac{S - S_o}{\tau_r}, \quad (61)$$

where now $D/D\tau = u^\mu{}_{;\mu}$. Then in a steady state

$$u^r \frac{dS}{dr} = -\frac{S - S_o}{\tau_r}. \quad (62)$$

The rest of the argument proceeds as before: we differentiate the angular momentum equation, solve for dS/dr , eliminate dS/dr from equation (62), and solve for S . We find

$$S = \frac{1}{1 - \tau_r u^r (2/r + d \ln F / dr)} \left(S_o + \frac{\rho \tau_r (u^r)^2}{F} \frac{d(l\eta)}{dr} \right). \quad (63)$$

We must now specify S_o .

The most natural form for the equilibrium value of the LRF shear stress is the Navier-Stokes value:

$$S_o = -2\rho\eta\nu\sigma_{(r)(\phi)}, \quad (64)$$

where $\nu = \alpha c_s r H_\theta$, following the usual α prescription. The calculation of $\sigma_{(r)(\phi)}$ is a lengthy, but important, matter that is left to the Appendix. The result is also complicated and left in the Appendix. Here we abbreviate it by

$$\sigma_{(r)(\phi)} \equiv \sigma \equiv \sigma_N + \sigma_L \frac{dl}{dr} + \sigma_V \frac{dV}{dr}. \quad (65)$$

⁶ We disagree with Abramowicz & Prasanna (1990), who argue that the viscous stress (indeed, the viscosity) vanishes at the horizon. Measured in the LRF, the viscous stress will not generally vanish at the horizon because the horizon is not in any way a special location from the point of view of the fluid, which falls freely through it. Transforming to the BLF, one finds that for general $t_{(a)(b)}$, $t^r{}_{\phi} = \gamma r \sqrt{\mathcal{A}\mathcal{D}} (t_{(r)(\phi)} + \beta_r \beta_\phi \gamma_r t_{(r)(r)})$. For geodesics $\gamma \sim \gamma_r \sim \mathcal{D}^{-1/2}$ near the horizon, so if $t_{(r)(\phi)}$ and $t_{(r)(r)}$ are finite at the horizon, so is $t^r{}_{\phi}$.

In the nonrelativistic limit, $\sigma = (1/2)r d\Omega/dr$, while in the thin disk limit $\sigma = -(3/4)r^{-3/2}\mathcal{D}/\mathcal{C}$ (Novikov & Thorne (1973)).⁷

Now we recover the full expression for the shear stress S . Substituting in equation (63) for S_o , we find

$$S = \frac{\rho\eta\nu}{1 - \tau_r u^r (2/r + d \ln F/dr)} \left\{ \frac{dl}{dr} \left(-2\sigma_L + \frac{(u^r)^2}{c_v^2} \frac{1}{F} \right) - 2\sigma_N - 2\sigma_V \frac{dV}{dr} + \frac{(u^r)^2}{c_v^2 F} \frac{d \ln \eta}{dr} \right\}. \quad (66)$$

The coefficient of dl/dr vanishes, and so there is a singular point in the flow, where $(u^r)^2 \approx c_v^2$.

4.3. Dissipation Function

The dissipation function Φ is best calculated in the LRF, where

$$\Phi = -t^{(a)(b)}\sigma_{(a)(b)} \quad (67)$$

Since most of the components of t vanish in the LRF, and the metric is Minkowski there, one finds

$$\begin{aligned} \Phi &= -2S\sigma \\ &= \rho\eta\nu \left(4\sigma^2 - 2\sigma \frac{(u^r)^2}{c_v^2 \eta f} \frac{d(l\eta)}{dr} \right) \end{aligned} \quad (68)$$

If $\sigma < 0$ and $d(l\eta)/dr > 0$ then Φ is positive.

It turns out that the dissipation function is not always positive in our solutions. In particular, σ sometimes changes sign close to the horizon, an effect first noticed by Anderson & Lemos (1988). Since the stress is not proportional to the shear rate, it need not change sign at the same point. The dissipation function then goes negative, indicating that the stress is transporting angular momentum outwards against the shear. In part this reflects the inadequacy of our phenomenological equation for the evolution of the viscous stress. In part this may be a physical effect, however, in the sense that small scale magnetic fields embedded in the flow are “wound up” by the shear and briefly unwind, reducing the internal

⁷ One can show that $-\sigma$ is the maximum growth rate for the Balbus-Hawley instability in a thin Kerr disk. The factor \mathcal{D}/\mathcal{C} varies from 1 at large radius to 4/3 at the last stable orbit. In the mechanical analogy for the Balbus-Hawley instability developed by Balbus & Hawley (1992) this result is unaffected by radial motions, to first order in the eccentricity.

energy of the fluid (into which we folded the magnetic energy). But it seems unlikely that this unwinding is fully reversible. As we shall see in the sample numerical solutions, this effect has no practical consequences since it only occurs close to the horizon, where the inflow time is short compared to the heating time and so the flow is nearly adiabatic.

5. Critical Points

The accretion flow must pass through two critical points. The first is the usual sonic point, which is made rather complicated by the presence of relativistic terms. The second is the “viscous point” that originates in the vanishing of the coefficient of dl/dr in the angular momentum equation. Here we develop explicit expressions for the associated boundary conditions.

Before proceeding, it is convenient to make two more approximations. These approximations eliminate terms that weakly couple the angular momentum equation to the other equations and enormously complicate the evaluation of the critical points. First, we replace $d \ln F/dr$ in equation (66) by $1/(r\gamma\sqrt{\mathcal{D}})$. This approximation is good to about 15% inside $r = 10$ and far better outside. Second, we replace $d \ln \eta/dr$ in equation (66) by $-(\eta - 1)/\eta r$. This approximation is good to about a factor of two. These terms are important mainly in the relativistic regime, where the shear stress is dynamically unimportant and the flow is nearly adiabatic.

5.1. Sonic Point

In order to obtain the sonic point conditions, we need to find an expression for the radial velocity gradient which involves no other derivatives. Therefore, we must find an explicit expression for the pressure derivative in (49). To accomplish this, we first gather together the conservation equations for particle number and energy (36) and (47), and the vertical equilibrium equation (53), and write them in differential form:

$$\frac{d \ln \rho}{dr} + \frac{d \ln H_\theta}{dr} + \frac{2}{r} + \frac{1}{1 - V^2} \frac{d \ln V}{dr} + \frac{1 - a^2/r}{r^2 \mathcal{D}} = 0 \quad (69)$$

$$(h(T) - 1) \frac{d \ln T}{dr} - \frac{d \ln \rho}{dr} = \frac{f\Phi}{\rho u^r T} \quad (70)$$

$$2 \frac{d \ln H_\theta}{dr} = (1 - Th(T)/\eta) \frac{d \ln T}{dr} - \frac{2}{r} - \frac{d \ln \nu_z^2}{dr}. \quad (71)$$

We have used $h(T) \equiv 1 + g(T) + Tdg/dT$, so that $d\eta/dr = h(T)dT/dr$, and $(1/\rho)\partial u/\partial T = h(T) - 1$. Notice that we have retained a term proportional to dH_θ/dr ; this term is assumed small, but we must retain it for consistency if we take equation (36) as our basic particle number conservation equation.

Using (71) to eliminate $d \ln H_\theta/dr$ from (36), we can solve for $d \ln \rho/dr$ and $d \ln T/dr$, and obtain $d \ln P/dr = d \ln \rho/dr + d \ln T/dr$. Substituting the result into (49), we obtain

$$\frac{V^2}{1-V^2} \frac{d \ln V}{dr} = f_r - \frac{T}{\eta} \left[f_1(T) \left(\frac{1}{2} \frac{d \ln \nu_z^2}{dr} - \frac{1}{1-V^2} \frac{d \ln V}{dr} - \frac{r-1}{r^2 \mathcal{D}} \right) + f_2(T) \frac{f\Phi}{\rho u^r T} \right], \quad (72)$$

where

$$f_1(T) \equiv \frac{h(T)}{h(T) - 1 + (1/2)(1 - Th(T)/\eta)}, \quad f_2(T) \equiv \frac{1 - (1/2)(1 - Th(T)/\eta)}{h(T) - 1 + (1/2)(1 - Th(T)/\eta)}. \quad (73)$$

In the nonrelativistic ($T \rightarrow 0$) limit, $f_1 = 2\gamma_0/(\gamma_0 + 1)$ and $f_2 = (\gamma_0 - 1)/(\gamma_0 + 1)$.

Finally, we must move all terms proportional to $d \ln V/dr$ from the right-hand to the left-hand side of this equation. This is more involved than it first appears because both Φ and $d \ln \nu_z^2/dr$ include terms proportional to $d \ln V/dr$. First, Φ can be simplified by substituting the shear stress S from (52) into (68), which allows us to write

$$\frac{f\Phi}{\rho u^r T} = \frac{2\sigma f(l\eta - j)}{FT}. \quad (74)$$

We then divide σ into a part which is proportional to dV/dr and a part which is not:

$$\sigma = \left[\sigma_V + \sigma_L \left(\frac{dl}{dr} \right)_V \right] \frac{dV}{dr} + \sigma_N + \sigma_L \left(\frac{dl}{dr} \right)_N, \quad (75)$$

where we have taken $dl/dr = (dl/dr)_N + (dl/dr)_V dV/dr$. The terms $(dl/dr)_N$ and $(dl/dr)_V$ are derived from (52) using the shear stress (66). Thus, the $d \ln V/dr$ part of the Φ term is

$$- \frac{f_2(T)}{\eta} \left(\sigma_V + \sigma_L \left(\frac{dl}{dr} \right)_V \right) \frac{2f(l\eta - j)V}{F} \frac{d \ln V}{dr}. \quad (76)$$

Following a similar procedure, we find that the $d \ln \nu_z^2/dr$ term has a $d \ln V/dr$ part

$$- \frac{Tf_1(T)}{2\eta} \left(\frac{d \ln \nu_z^2}{dr} \right)_V \frac{dV}{dr} = - \frac{Tf_1(T)V}{\eta \nu_z^2} \left[\frac{l - \mathcal{E}a^2\Omega}{r^4} \left(\frac{dl}{dr} \right)_V - \frac{\mathcal{E}a^2}{r^4} \left(\frac{d\mathcal{E}}{dr} \right)_V \right] \frac{d \ln V}{dr}. \quad (77)$$

Solving for $d \ln V/dr$, we obtain

$$\frac{d \ln V}{dr} = \frac{N_s}{D_s}, \quad (78)$$

where

$$N_s = f_r - \frac{Tf_1(T)}{\eta} \left[\left(\frac{1}{2} \left(\frac{d \ln \nu_z^2}{dr} \right)_N - \frac{r-1}{r^2 \mathcal{D}} \right) \right] - \frac{f_2(T)}{\eta} \left(\sigma_N + \sigma_L \left(\frac{dl}{dr} \right)_N \right) \frac{2f(l\eta - j)}{F}, \quad (79)$$

and

$$D_s = \frac{V^2}{1-V^2} + \frac{Tf_1(T)}{\eta} \left(\frac{V}{2} \left(\frac{d \ln \nu_z^2}{dr} \right)_V - \frac{1}{1-V^2} \right) + \frac{f_2(T)}{\eta} \left(\sigma_V + \sigma_L \left(\frac{dl}{dr} \right)_V \right) \frac{2f(l\eta - j)V}{F}. \quad (80)$$

At the sonic point $N_s = D_s = 0$. In the nonrelativistic limit the condition $D_s = 0$ reduces to $V^2 = c_s^2 2\gamma_0 / (\gamma_0 + 1)$, in agreement with NKH.

5.2. Viscous Point

The viscous point conditions are obtained by solving the angular momentum equation (52) for dl/dr . We obtain

$$\frac{dl}{dr} = \frac{N_v}{D_v} \quad (81)$$

where

$$N_v = \frac{[1 - \tau_r u^r (2/r + d \ln F/dr)] V \mathcal{D}^{1/2}}{F \eta \nu (1 - V^2)^{1/2}} + 2\sigma_N + 2\sigma_V \frac{dV}{dR} - \frac{(u^r)^2}{c_v^2 F} \frac{d \ln \eta}{dr}. \quad (82)$$

and

$$D_v = -2\sigma_L + \frac{(u^r)^2}{c_v^2 F} \quad (83)$$

At the viscous point $N_v = D_v = 0$. The conditions $D_v = 0$ is equivalent to

$$\frac{V^2}{c_v^2} = \gamma(\mathcal{A}/\mathcal{D})^{1/2} (1 - V^2) (\mathcal{E} - l\Omega). \quad (84)$$

We take $c_v^2 = \alpha c_s^2$, and since $\alpha < 1$ the viscous point will generally be located well outside the sonic point.

6. Example Numerical Solution

In this section we find a typical numerical solution and use it to study the importance of various relativistic terms, to check our approximations, and evaluate the robustness of the input physics. More precisely, we have solved the system of equations (39), (47), (49) and (52) numerically, using a relaxation scheme (see Popham & Gammie (1997) for more

details). We have set $f = 1$ (zero cooling), $\alpha = 0.1$, and the rotation parameter of the black hole $a = 0$.

The system is subject to five boundary conditions that allow us to solve the first order differential equations for V, l, ρ, T and for the eigenvalue j over a domain that extends from just outside the event horizon to $r = 2 \times 10^4 GM/c^2$. Two boundary conditions are provided by equations (79) and (82), which ensure the solution passes smoothly through the sonic and viscous points, respectively. Two additional boundary conditions fix l and T at the outer edge of the solution (V must be determined self-consistently there). We set $T_{out} = 1.67 \times 10^{-5}$ and $l_{out} = 57.75$. These values are taken from the self-similar solution of Narayan & Yi (1994). NKH have shown that global solutions with, e.g., thin disk outer boundary conditions, rapidly approach this self-similar solution, which then spans many decades in radius. Consistent with this, we find that the character of the solution at $r \lesssim 10^2$ is insensitive to the outer boundary conditions. A final boundary condition is obtained by normalizing the density so that the rest-mass accretion rate $\dot{M} = 1$.

The run of the basic variables V, l, ρ, T with radius is shown in Figure 1. ⁸ The upper left panel shows V , and the arrows indicate the location of the sonic point at $r_s = 6.41$ (slightly outside the last stable circular orbit at $r = 6$) and the viscous point at $r_v = 28.2$. At the viscous point $V \approx 0.3c_s$ and so it lies far outside the sonic point. The solution is, however, insensitive to the precise definition of c_ν . For example, setting $c_\nu = 0.5c_s$ changes j by less than 4%. The solution reaches $V = 1$ at the event horizon, which is located at $r = 2$.

The upper right panel in Figure 1 shows l (heavy solid line), $l\eta$ (dashed line), and the eigenvalue $j = 2.62$ (dotted line). Recall that $l\eta$, rather than l , is conserved in the absence of viscous torques, and that $\dot{M}j$ is the total inward flux of angular momentum. The difference $l\eta - j$ is proportional to the shear stress; in this case the difference is a small positive number at the horizon. The lower left panel shows density, which very nearly follows a power law $r^{-3/2}$ over the whole solution. The lower right panel shows the temperature, which reaches a maximum of 0.067, corresponding to a sound speed $c_s = 0.28c$. As we shall see, the maximum temperature and density of the solution change significantly with black hole rotation.

The run of some important dynamical quantities is shown in Figure 2. The upper left panel shows the absolute value of the shear rate in the LRF. The shear changes sign at $r \approx 3$. Also shown is the thin disk approximation to the shear rate, equation (A6), which

⁸Physical units may be recovered as follows: radial velocity is Vc , angular momentum is lGM/c , density is $\rho\dot{M}G/c^3$ (since the mass accretion rate is normalized to 1), and temperature is $T\bar{m}c^2/k$.

lies too close to the actual shear rate to distinguish it on this plot. The maximum difference between the two is about one part in 10^3 . The upper right panel shows the causal shear stress as a solid line and the equilibrium shear stress S_0 (proportional to the shear rate, see equation [64]) as a dashed line. The causal stress is relaxing toward S_0 but the fluid is also flowing inwards toward regions of larger shear, so the causal stress always lies slightly below S_0 . The lower left panel shows H_θ . The vertical averaging approximation is accurate to of order $d \ln H_\theta / d \ln R$, which is largest at the horizon. The lower right panel shows $\Omega \equiv u^\phi / u^t$. For $a = 0$ we must have $\Omega = 0$ at the horizon, so Ω goes through a maximum at $r \approx 3$. This is consistent with our statement that the shear rate in the LRF is very nearly proportional to $d\Omega/dr$.

Thermodynamic quantities are shown in Figure 3. These are the relativistic enthalpy η , the pressure p , the entropy S (minus its value at the outer edge), and the dissipation function Φ . As discussed earlier, the dissipation function goes negative at $r \approx 3.0$, where the shear changes sign. This is an inevitable result of our causal viscosity prescription. It has little practical significance, however, since, as can be seen from Figure 3, the flow is nearly isentropic at $r < 3.0$. This is because the radial inflow time becomes short compared to the heating time.

This work contains two new physical ingredients as compared to NKH: a causal viscosity prescription, and a full treatment of relativistic effects. We can evaluate the influence of each by solving a simplified version of our equations which retains our causal viscosity formulation, but eliminates all relativistic corrections and terms and adopts the Paczyński potential used by NKH. We can compare the NKH solution and the causal solution to find the effects of the causal viscosity, and we can compare the causal solution and the full, relativistic solution to find the effect of properly including relativity.

The results are displayed in Figure 4, which shows the basic variables V, l, ρ, T in each of the three solutions: the fully relativistic solution (heavy solid line), the causal solution (long dashed line) and the NKH solution (dotted line). Also shown in the angular momentum plot is a short dashed line, which is the angular momentum of a thin disk (inside $r = 6$ the angular momentum is that of the last stable orbit). Before continuing with the comparison, notice that all the ADAF solutions lie below the thin disk solution in angular momentum—evidently they are all “sub-Keplerian”.

Remarkably, the relativistic solution, causal solution, and NKH solution are very similar at $r \gtrsim 10$. This suggests that the solutions are robust in the sense that significant changes in the input physics cause only small changes in the solution. One can also check the robustness of the shear stress model by changing the definition of c_ν^2 . If we set $c_\nu^2 = c_s^2$ (rather than αc_s^2) we find that the values of the basic dependent variables change by no

more than 5.9% at the inner boundary. Again, this suggests that the solution is robust.

What is the effect of the causal viscosity? The comparison of the causal solution and the NKH equations is not perfect because NKH take $\nu_z^2 = \Omega_K^2$ (which diverges at $r = 2$), while we take $\nu_z^2 = \Omega^2$. The outcome of combining these two changes is to lower the angular momentum slightly and decrease the radial velocity (therefore increasing the density) in comparison to NKH. What is the effect of properly including the relativity? The most obvious effect is in the radial velocity, which diverges at $r = 2$ in the causal solution because the potential gradient diverges there. This causes the density and temperature to go through a maximum and then decline to zero at $r = 2$. In the relativistic solution, by contrast, the density and temperature increase monotonically in to the horizon. The next most obvious effect is in the angular momentum profile, which is significantly lower at the horizon in the relativistic solution than in the causal solution. This is due to our retention of relativistic enthalpy terms in the angular momentum equation; the angular momentum per unit rest mass is $l\eta$ rather than l .

The similarity of all three ADAF solutions in Figure 4 should not lead one to conclude that relativistic effects are not important. Figure 5 shows the effect of varying a from -0.999 to 0 to 0.999 . The temperature at the horizon increases from 0.067 when $a = 0$ to 0.363 when $a = 0.999$, while the density increases from 0.11 at $a = 0$ to 1.29 at $a = 0.999$. These changes suggest the possibility that ADAF emission properties may depend strongly on black hole rotation. We defer a more detailed discussion of the effect of black hole rotation to Popham & Gammie (1997).

We can now check our approximations for self-consistency. Vertical averaging cannot be checked directly, but the smallness of $|d \ln H_\theta / d \ln r|$ compared to 1 is a rough test of its validity (this also tests the validity of our vertical equilibrium approximation). The maximum in $|d \ln H_\theta / d \ln r|$ is 0.697 at the horizon and much smaller outside (see Figure 2). The situation would be improved if the scale height were allowed to evolve dynamically, so that H_θ could “freeze out” near the horizon.

We have also dropped viscous accelerations in the radial momentum equation. One would expect that the viscous term is of order α compared to the dominant terms, and a direct check confirms this. The viscous term generally produces an outward directed acceleration, although in the inner parts of those solutions where the shear changes sign (generally when $a \lesssim 0.7$) it produces an inward acceleration.

We made two additional approximations prior to deriving the sonic point conditions: (1) we set $d \ln F / dr \simeq 1 / (r\gamma\sqrt{\mathcal{D}})$; (2) $d \ln \eta / dr \simeq -(\eta - 1) / \eta r$. We have checked these approximations by multiplying the approximated term by 0.5 and examining the effect on

the solution. For approximation (1) we find the largest fractional change is 2.7% in T at the innermost radius. For (2) we find the largest fractional change is 0.2% in l at the innermost radius. This shows that the approximations, whose accuracy was discussed at the beginning of §5, do not affect the solution very much.

Finally, how important are the relativistic thermodynamic terms (η and g) that we have worked so hard to include? The η term turns out to be quite important, particularly for holes with rapid prograde rotation. When $a = 0.999$, the maximum value of η is 2.26; this implies substantial corrections in the angular momentum and radial momentum equations. The relativistic equation of state is somewhat less important; the maximum ratio of g to $1/(\gamma_o - 1)$ (the nonrelativistic value) is 1.10.

7. Summary

We have written down and solved equations describing optically thin, advection dominated flows in the Kerr metric. Our physical description of the flow includes a causal prescription for the viscosity, and does not require the application of a boundary condition at the event horizon. We solve the energy equation assuming that a constant fraction of the dissipated energy is advected. We have also included certain relativistic terms that have been neglected in some earlier treatments; most importantly, we do not assume that the relativistic enthalpy η is unity. We will present a detailed survey of solutions for various choices of parameters in an upcoming paper (Popham & Gammie (1997)). These solutions, when coupled with a detailed description of the cooling processes and a photon transport scheme, will allow us to produce model spectra for advection dominated systems.

We are grateful to R. Narayan for helping to initiate this project and for his support, insight and encouragement, and to J.-P. Lasota and W. Press for helpful discussions. This work was supported by NASA grant NAG 5-2837 and NSF grant AST 9423209.

A. Shear Rate in the Local Rest Frame

We want $\sigma_{(r)(\phi)}$, which is the shear rate measured in the local rest frame (LRF). Using the basis vectors for the LRF,

$$\sigma_{(r)(\phi)} = e^\mu_{(r)} e^\nu_{(\phi)} \sigma_{\mu\nu}, \tag{A1}$$

where $\sigma_{\mu\nu}$ is given by equation (33). We must then calculate many of the pieces of $\sigma_{\mu\nu}$, although our task is simplified a bit because

$$e^\mu{}_{(a)}u_\mu = \delta_{(a)}^{(t)}, \quad (\text{A2})$$

since $e^\mu{}_{(t)}$ is parallel to u^μ , and the basis vectors are orthonormal. Along the way we find

$$\begin{aligned} u_{t;t} &= -\frac{\beta_r\gamma_r\sqrt{\mathcal{D}}}{r^2} \\ u_{t;r} &= -\frac{d\mathcal{E}}{dr} + u_{r;t} \\ u_{t;\phi} &= \frac{a\beta_r\gamma_r\sqrt{\mathcal{D}}}{r^2} \\ u_{r;t} &= (1 - a\Omega)\frac{\gamma}{r^2}\sqrt{\frac{\mathcal{A}}{\mathcal{D}}} \\ u_{r;r} &= \frac{du_r}{dr} + \beta_r\gamma_r(1 - a^2/r) \\ u_{r;\phi} &= -\frac{\gamma}{r^2}\sqrt{\frac{\mathcal{A}}{\mathcal{D}}}(a - a^2\Omega + r^3\Omega) \\ u_{\phi;t} &= u_{t;\phi} \\ u_{\phi;r} &= \frac{dl}{dr} + u_{r;\phi} \\ u_{\phi;\phi} &= r\beta_r\gamma_r\sqrt{\mathcal{D}}(1 - a^2/r^3). \end{aligned} \quad (\text{A3})$$

Using equation (17),

$$\begin{aligned} \frac{d\mathcal{E}}{dr} &= \frac{V\gamma_r^4}{\gamma}\sqrt{\frac{\mathcal{D}}{\mathcal{A}}}\frac{dV}{dr} + \Omega\frac{dl}{dr} - \frac{l\omega}{r\mathcal{A}}(3 + a^2/r^2) + \frac{\gamma(1 - a^2/r)}{r^2\sqrt{\mathcal{A}\mathcal{D}}} + \\ &\quad \frac{\gamma\sqrt{\mathcal{D}}a^2(1 + 3/r)}{r^3\mathcal{A}^{3/2}} - \frac{l^2(1 - a^2/r^3)}{r^3\mathcal{A}^2\gamma}\sqrt{\frac{\mathcal{D}}{\mathcal{A}}} \end{aligned} \quad (\text{A4})$$

Assembling the results and transforming to the LRF, we find

$$\begin{aligned} \sigma_{(r)(\phi)} &= -\frac{lV\gamma_r^4}{2r\gamma}\sqrt{\frac{\mathcal{D}}{\mathcal{A}}}\frac{dV}{dr} + \frac{\mathcal{E} - l\Omega}{2r}\frac{dl}{dr} - \frac{l^2\omega(3 + a^2/r^2)}{2r^2\gamma_r^2\mathcal{A}} - \frac{1}{2}\gamma_\phi^2\omega(3 + a^2/r^2) \\ &\quad + \frac{\gamma_\phi l}{\gamma_r}\sqrt{\frac{\mathcal{A}}{\mathcal{D}}}\left(\frac{1}{r^3} - \frac{\mathcal{D}(1 - a^2/r^3)}{\mathcal{A}^2r^2} - \omega^2(2 + a^2/r^2 + a^2/r^3)\right) \\ &\quad + \frac{l^2\omega(3 + a^2/r^2)}{2r^2\mathcal{A}} - \frac{l\gamma(1 - a^2/r)}{2r^3\sqrt{\mathcal{A}\mathcal{D}}} - \frac{l\gamma\sqrt{\mathcal{D}}a^2(1 + 3/r)}{2r^4\mathcal{A}^{3/2}} + \frac{l^3(1 - a^2/r^3)}{2r^4\mathcal{A}^2\gamma}\sqrt{\frac{\mathcal{D}}{\mathcal{A}}}. \end{aligned} \quad (\text{A5})$$

For a relativistic thin disk, this reduces to the remarkably simple expression

$$\sigma_{(r)(\phi)} = \frac{1}{2}r\mathcal{A}\gamma_\phi^2\frac{d\Omega}{dr} \quad (\text{THIN DISK}) \quad (\text{A6})$$

(Novikov & Thorne (1973)). Obviously this reduces correctly to the nonrelativistic limit. Remarkably, this thin disk expression for σ lies within a fraction of a percent of the full LRF shear stress in our advection dominated solutions.

For cold, geodesic flow ($l = \text{const.}$, $\mathcal{E} = \text{const.}$) onto a nonrotating hole, σ reduces to

$$\sigma_{(r)(\phi)} = \frac{\gamma_{\phi} l}{\gamma_r \sqrt{\mathcal{D}} r^2} (1 - 3/r). \quad (a = 0, \text{GEODESIC}) \quad (\text{A7})$$

This case is simple enough to be checked by hand. It shows the shear reversal at $r = 3$ discovered by Anderson & Lemos (1988) and discussed in detail by Abramowicz & Prasanna (1990).

REFERENCES

- Abramowicz, M.A., Chen, X., Granath, M., & Lasota, J.-P. 1997, ApJ, 471, 762 (ACGL)
- Abramowicz, M.A., Chen, X., Kato, S., Lasota, J.-P., & Regev, O. 1995, ApJ, 438, L37
- Abramowicz, M. A., Czerny, B., Lasota, J.-P., & Szuszkiewicz, E. 1988, ApJ, 332, 646
- Abramowicz, M.A., Lanza, A., & Percival, M.J. 1997, ApJ479, 179 (ALP)
- Abramowicz, M. A., & Prasanna, A. R. 1990, MNRAS, 245, 720
- Anderson, M. R., & Lemos, J.P.S. 1988, MNRAS, 233, 489
- Balbus, S.A., Gammie, C.F., & Hawley, J.F. 1994, MNRAS, 271, 197
- Balbus, S.A., & Hawley, J.F. 1991, ApJ, 376, 214
- Balbus, S.A., & Hawley, J.F. 1992, ApJ, 392, 662
- Bardeen, J.M., & Petterson, J.A. 1985, ApJ, 195, L65
- Bardeen, J. M., Press, W. H., & Teukolsky, S. A. 1972, ApJ, 178, 347 (BPT)
- Begelman, M. C., & Meier, D. L. 1982, ApJ, 253, 873
- Carter, B. 1968, Phys. Rev., 174, 1559
- Chakrabarti, S. 1996, ApJ, 471, 237
- Chen, X., Abramowicz, M. A., & Lasota, J.-P. 1997, ApJ, 476, 61

- Chen, X., Abramowicz, M. A., Lasota, J.-P., Narayan, R., & Yi, I. 1995, *ApJ*, 443, L61
- Ellis, G.F.R., in *General Relativity and Cosmology 1971*, ed. B.K. Sachs (New York: Academic), p. 104
- Israel, W., in *General Relativity: Papers in Honor of J.L. Synge 1972*, ed. L. O’Raifeartaigh (Oxford: Clarendon), p. 201
- Kato, S. 1994, *PASP*, 46, 589
- Kato, S., & Inagaki, S. 1994, *PASP*, 46, 289
- Kumar, S., & Pringle, J.E., 1985, *MNRAS*, 213, 435
- Lasota, J.-P. 1994, in *Theory of Accretion Disks 2*, Duschl et al., eds (Dordrecht: Kluwer), p. 341
- Misner, C.W., Thorne, K.S., & Wheeler, J.A. 1973, *Gravitation* (New York: Freeman)
- Muchotrzeb, B., & Paczyński, B. 1982, *Acta Astronomica*, 32, 1
- Narayan, R. 1992, *ApJ*, 394, 261
- Narayan, R. 1997, in *Proceedings of IAU Colloquium 163, Accretion Phenomena and Related Objects*, A. S. P. Conference Series, eds. D. T. Wickramasinghe, L. Ferrario, & G. V. Bicknell, in press (astro-ph/9611113)
- Narayan, R., Kato, S., & Honma, F. 1997, *ApJ*, 476, 49
- Narayan, R., Loeb, A., & Kumar, P. 1994, *ApJ*, 431, 359
- Narayan, R., & Popham, R. 1993, *Nature*, 362, 820
- Narayan, R., & Yi, I. 1994, *ApJ*, 428, L13
- Narayan, R., & Yi, I. 1995, *ApJ*, 444, 231
- Narayan, R., & Yi, I. 1995, *ApJ*, 452, 710
- Novikov, I., & Thorne, K.S. 1973, in *Black Holes*, ed. DeWitt, C. & Dewitt, B.S., (New York: Gordon & Breach), p. 343
- Paczyński, B., & Bisnovatyi-Kogan, G. 1981, *Acta Astronomica*, 31, 283
- Paczyński, B., & Wiita, P. 1980, *A&A*, 88, 23

- Papaloizou, J.C.B., & Szuszkiewicz, E. 1994, MNRAS, 268, 29
- Peitz, J., & Appl, S. 1997, MNRAS, 286, 681 (PA)
- Popham, R., & Gammie, C.F. 1997, ApJ, in preparation
- Rees, M., Begelman, M.C., Blandford, R.D., & Phinney, E.S. 1982, Nature, 295, 17
- Riffert, H., & Herold, H. 1995, ApJ, 450, 508
- Service, A. T. 1986, ApJ, 307, 60
- Shakura, N. I., & Sunyaev, R. A. 1973, A&A, 24, 337
- Thorne, K.S. 1974, ApJ, 191, 507

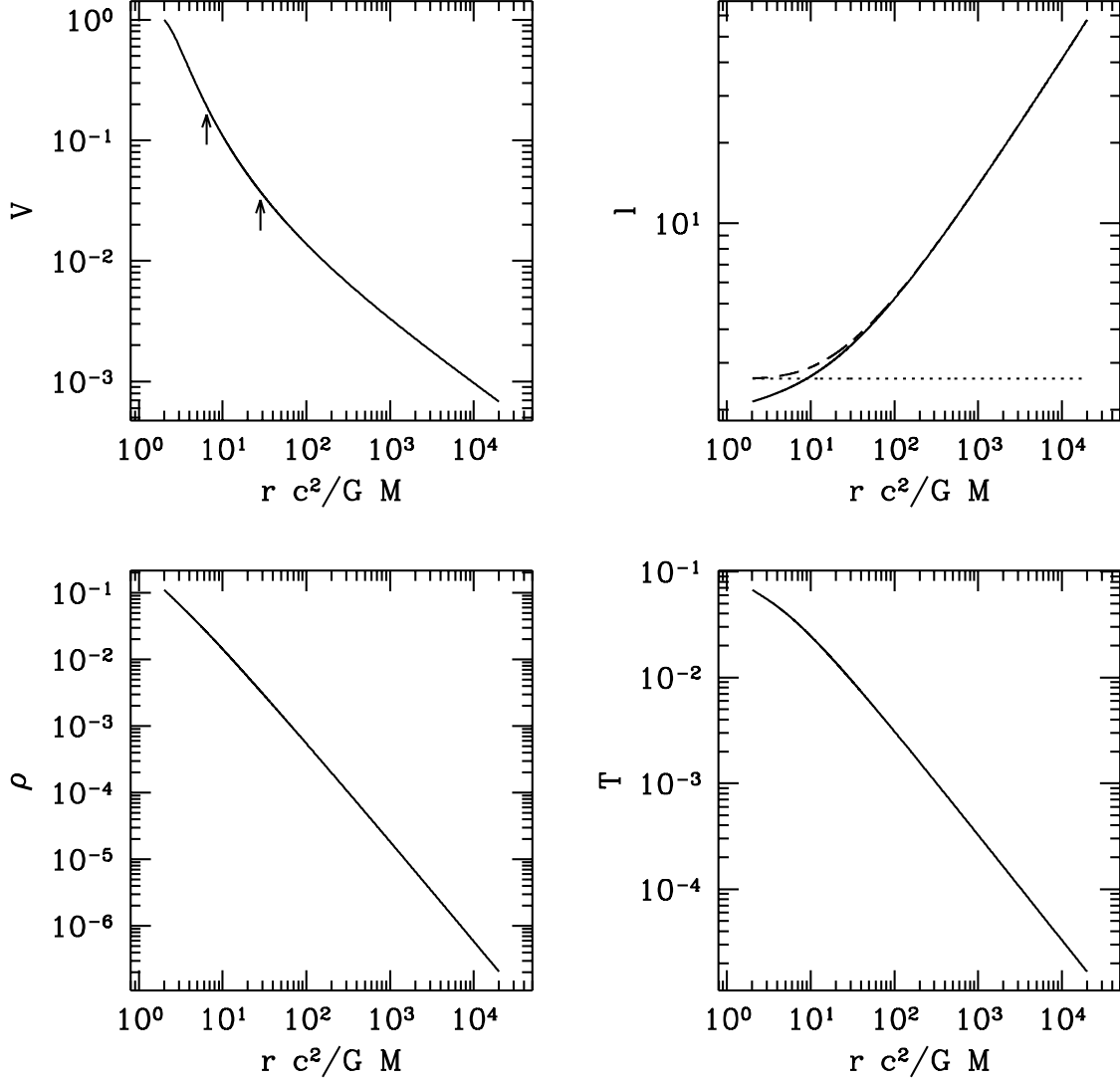


Fig. 1.— Solution to the full relativistic equations with $a = 0$, $\alpha = 0.1$, $f = 1$. The upper left panel shows the radial velocity V measured in the CRF. The arrows show the location of the sonic and viscous critical points. The upper right panel shows the angular momentum l (solid line) as well as $l\eta$ (dashed line) and j (dotted line). The lower left panel shows density and the lower right panel shows dimensionless temperature T .

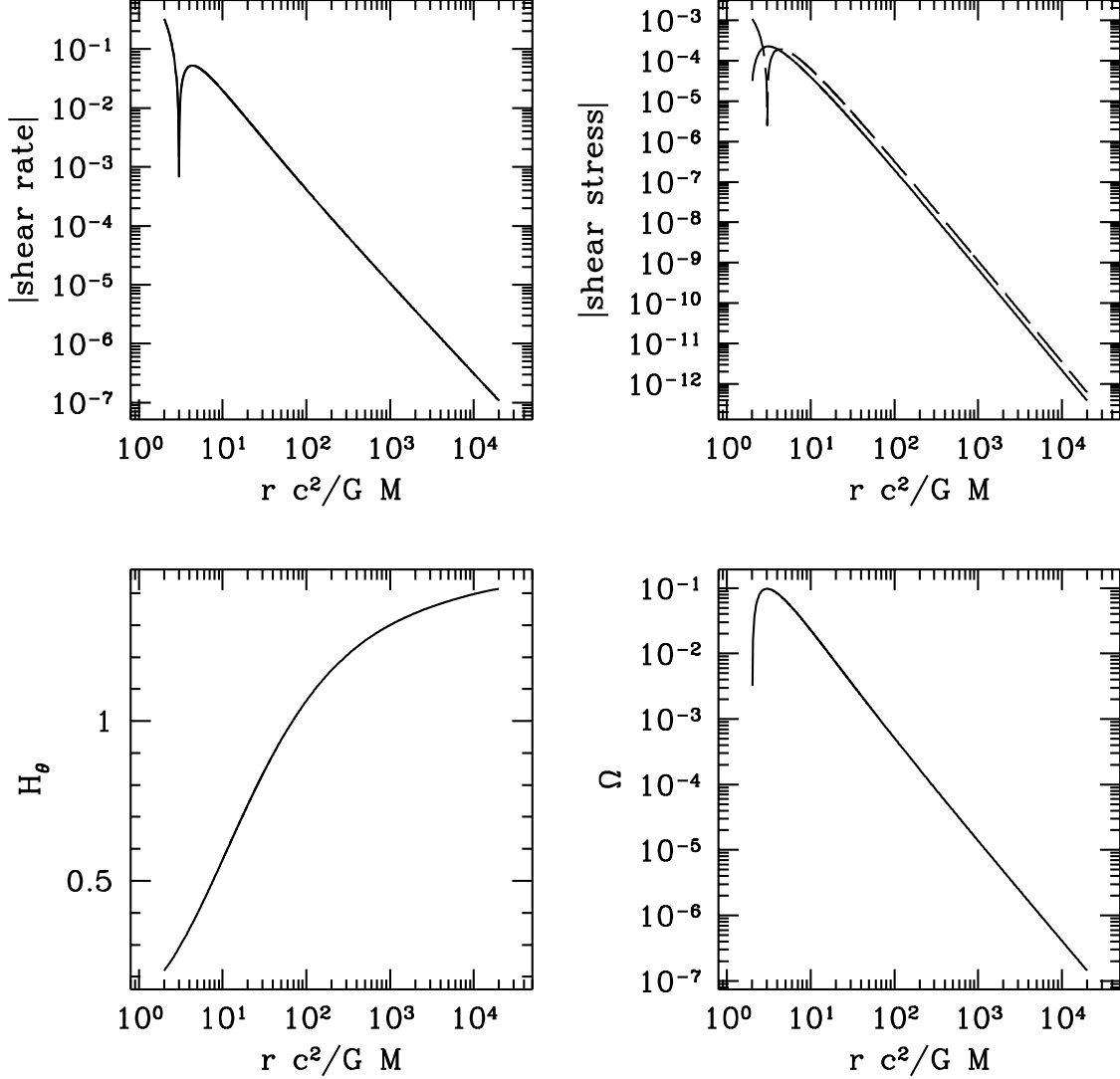


Fig. 2.— Dynamical quantities in the $a = 0$ solution. The upper left panel shows the shear rate measured in the LRF. The approximate formula for the shear rate, based on the thin disk shear, is also shown but is too close to distinguish on this plot. The upper right panel shows both the causal shear stress (solid line) and the acausal (Navier-Stokes) version, which is proportional to the shear rate (dashed line). The lower left panel shows the angular scale of the flow H_θ , while the lower right shows the angular frequency $\Omega = u^\phi/u^t$.

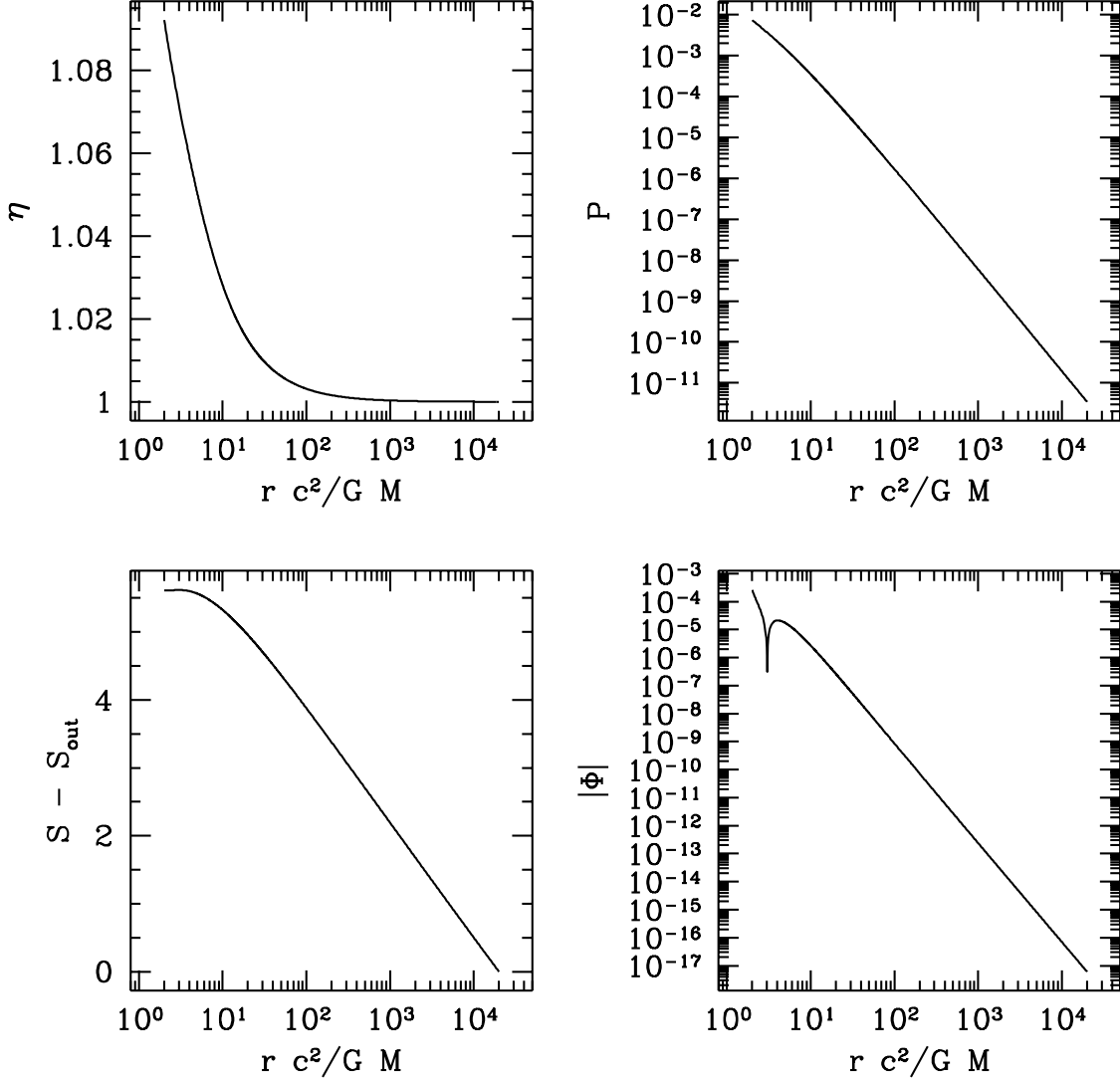


Fig. 3.— Thermodynamic quantities in the $a = 0$ solution. The upper left panel shows the relativistic enthalpy η , the upper right panel shows pressure, the lower left entropy, and the lower right the absolute value of the dissipation function. The dissipation function changes sign at $r \simeq 3$.

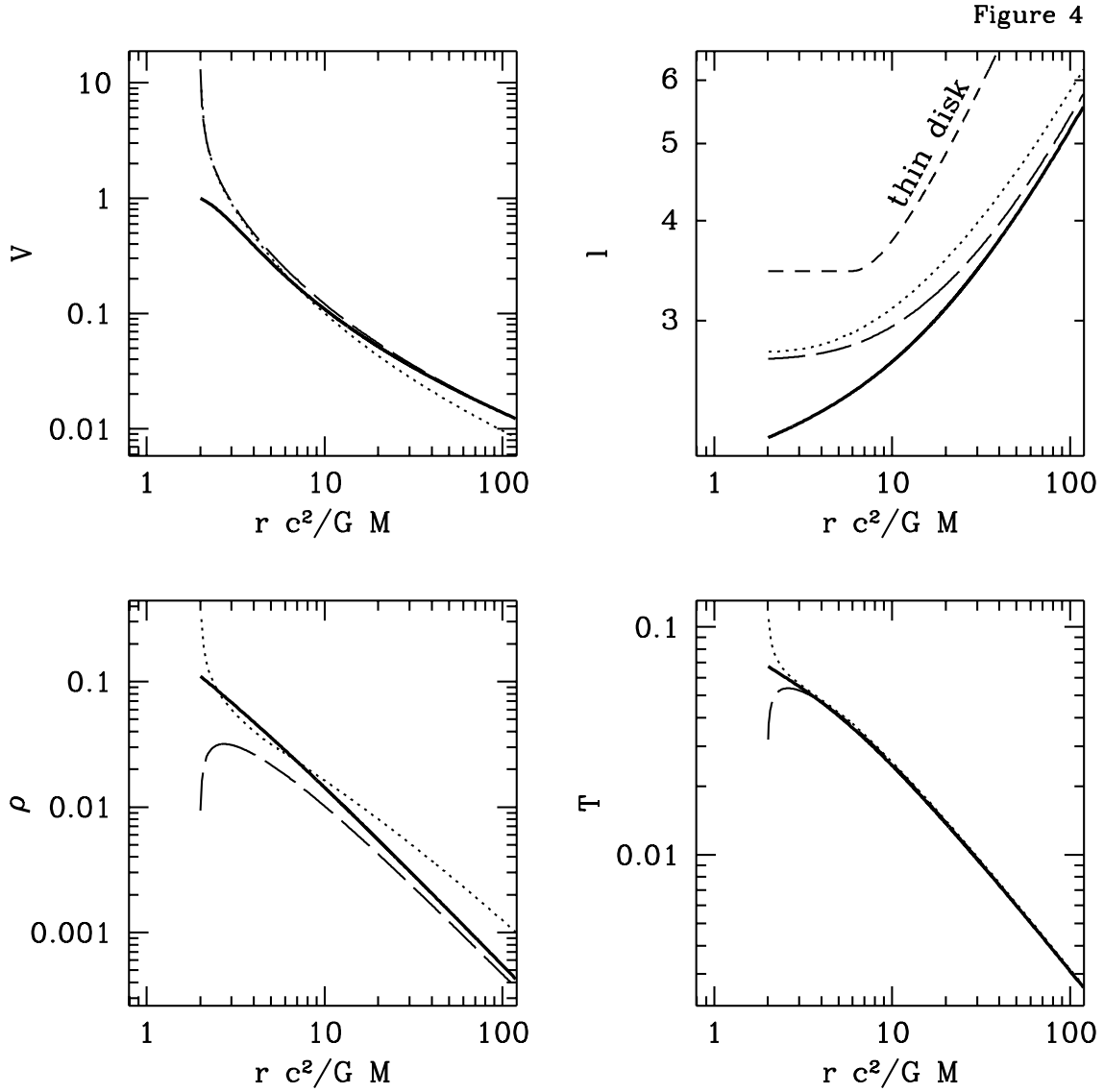


Fig. 4.— A comparison of various ADAF solutions: the relativistic solution (heavy solid line); a solution of the causal nonrelativistic limit of the relativistic equations (long dashed line); the NKH solution (dotted line); and the thin disk angular momentum distribution (short dashed line).

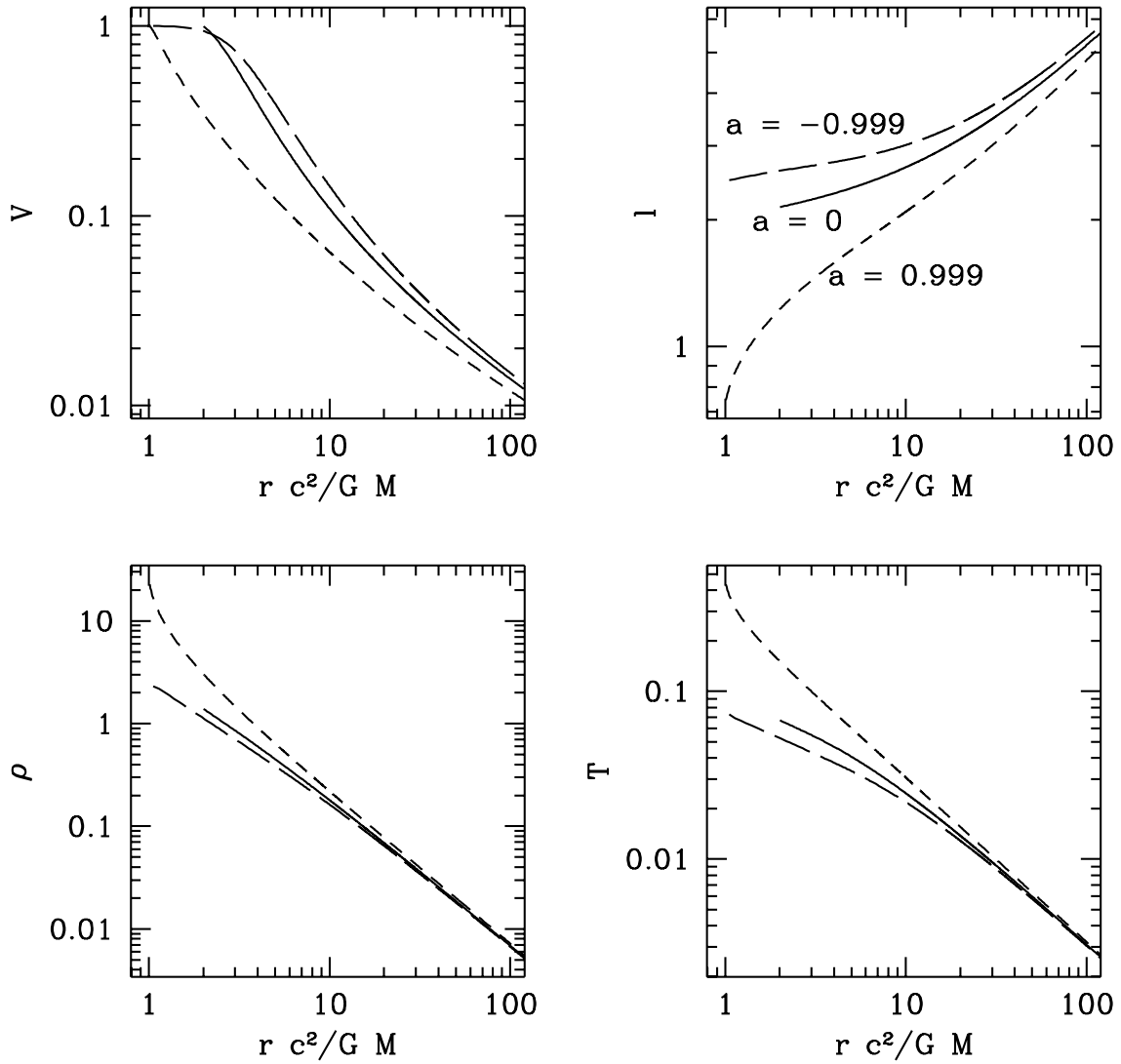


Fig. 5.— A comparison of the relativistic solution for different black hole angular momenta. Shown are solutions for $a = 0$ (solid line), $a = -0.999$ (long dashed line) and $a = 0.999$ (short dashed line).